INTERNATIONAL JOURNAL FOR NUMERICAL METHODS IN FLUIDS
Int. J. Numer. Meth. Fluids 2008; **57**:31–45
Published online 13 September 2007 in Wiley InterScience (www.interscience.wiley.com). DOI: 10.1002/fld.1610

A hybrid vortex method for the simulation of three-dimensional flows

Wei Li*,† and Marco Vezza

Department of Aerospace Engineering, University of Glasgow, Glasgow G12 8QQ, U.K.

SUMMARY

This paper presents an integral vorticity method for solving three-dimensional Navier–Stokes equations. A finite volume scheme is implemented to solve the vorticity transport equation, which is discretized on a structured hexahedral mesh. A vortex sheet algorithm is used to enforce the no-slip boundary condition through a vorticity flux at the boundary. The Biot–Savart integral is evaluated to compute the velocity field, in conjunction with a fast algorithm based on multipole expansion. This method is applied to the simulation of uniform flow past a sphere. Copyright © 2007 John Wiley & Sons, Ltd.

Received 5 March 2007; Revised 16 July 2007; Accepted 19 July 2007

KEY WORDS: vortex method; finite volume method; three-dimensional flow; fast summation; sphere flow

1. INTRODUCTION

Computational fluid dynamic (CFD) methods have been developed for several decades, providing an efficient tool for the analysis of many fundamental and practical fluid dynamics problems. Various numerical techniques have been employed to solve the Navier–Stokes equations that govern viscous fluid flow, by using the Euler description, in which the truncated domain of the entire flow region is overlaid by a grid system. Despite the huge success on the simulation of complex fluid flow, standard CFD methods that rely on solving equations of primitive variables, the velocity and pressure, are susceptible to excessive numerical dissipation of vorticity. If not controlled, this dissipation ultimately leads to an enhanced spreading of the vorticity support and a loss of circulation of the vortex structures.

Lagrangian vorticity methods, on the other hand, follow an alternative approach, in which the vorticity–velocity form of Navier–Stokes equations only needed to be solved within the limited

*Correspondence to: Wei Li, Department of Aerospace Engineering, University of Glasgow, Glasgow G12 8QQ, U.K.
†E-mail: lwei@aero.gla.ac.uk

Contract/grant sponsor: EPSRC

vorticity-containing regions, so that they appear to be efficient and self-adaptive [1–4]. Since the nonlinear convection term is included in the vorticity time derivative, Lagrangian vorticity methods exhibit little or no numerical dissipation. However, despite these advantages, Lagrangian vorticity methods experience some challenging problems that hinder their application in general fluid dynamics. One of these problems is the computational cost in evaluating the velocity of vortices *via* the Biot–Savart law. In this process, the integration used to compute velocity with N vortices is $O(N^2)$, and is therefore quite slow and usually prohibitive for large N. This situation has been improved by introducing several acceleration methods, such as the fast summation algorithm, which is based on the expansion of the kernel function in the Biot–Savart formula [5, 6]. A hierarchical structure is commonly used in these acceleration methods such that the particle–particle interaction is converted to the particle–group or group–group interaction, with the overall computational complexity reduced from $O(N^2)$ to $O(N \ln N)$ or $O(N)$.

Another problem associated with Lagrangian vorticity methods is the simulation of viscous diffusion. Instead of the random walk approach that has a shortcoming of slow-convergence rate, a variety of deterministic methods have been developed over the last two decades. In one of these methods, the concept of diffusive velocity is introduced by defining an equivalent convection velocity for the diffusion process. The application of this method to the flow around a circular cylinder and aerofoil [7] shows that smoother results can be obtained if the vortex particles strictly overlap. Another deterministic method is the particle strength exchange scheme [8], in which the circulations associated with the vortex particles irregularly distributed in the flow are redistributed either by the use of an integral representation for the Laplacian operator or a more complicated formula given in [9]. However, after a period of evolution, the vortex particle distribution may become uneven, thus destroying the overlapping condition, which necessitates a complicated remeshing process [8, 10].

The current paper introduces a new hybrid approach to resolve some of the remaining difficulties associated with the Lagrangian vorticity methods. Instead of employing overlapping vortex particles/blobs, a hexahedral grid system is introduced to solve the three-dimensional incompressible Navier–Stokes equations using the finite volume method. A modified Biot–Savart formula is used to calculate the velocity within the parts of the grid system where non-zero vorticity exists. Owing to the nature of the finite volume method, this hybrid approach can guarantee the conservation of the vorticity and mass within the entire flow domain. The use of hexahedral elements requires a proper numerical integration procedure for calculating the velocity. This has been accomplished by using closed-form formulas proposed by Suh [11] with essential completion from this study.

2. PROBLEM STATEMENT

The Navier–Stokes equations governing incompressible flow can be written in primitive variable (velocity–pressure) form as

$$\frac{\partial}{\partial t}\mathbf{u} + \mathbf{u} \cdot \nabla \mathbf{u} = -\frac{1}{\rho}\nabla p + \nu \nabla^2 \mathbf{u} \tag{1}$$

$$\nabla \cdot \mathbf{u} = 0 \tag{2}$$

where $\mathbf{u}(x, t)$ is the velocity field and ν is the kinematic viscosity.

DOI: 10.1002/fld

Taking the curl of Equation (1) yields the unsteady vorticity transport equation

$$\frac{\partial}{\partial t}\boldsymbol{\omega} + \mathbf{u}\cdot\nabla\boldsymbol{\omega} - \boldsymbol{\omega}\cdot\nabla\mathbf{u} = \nu\nabla^2\boldsymbol{\omega} \tag{3}$$

for the vorticity field $\boldsymbol{\omega}(x,t) = \nabla\times\mathbf{u}(x,t)$. In viscous flow, a non-slip boundary condition must be satisfied on solid surfaces, including a Dirichlet condition on the normal component of $\boldsymbol{\omega}$ [10] (as the tangential derivatives of the velocity vanish at the wall),

$$\omega_n = \boldsymbol{\omega}\cdot\mathbf{n} = 0 \tag{4}$$

and a Neumann condition on the two tangential components of $\boldsymbol{\omega}$ (cancellation of the tangential components of the slip velocity at the wall).

The force $\mathbf{F}$ on an immersed solid body with surface $\mathbf{S}$ can be calculated by the sum of the pressure and viscous shear forces as

$$\mathbf{F} = -\int_S (p\mathbf{n} + \mu\mathbf{n}\times\boldsymbol{\omega})\,\mathrm{d}s \tag{5}$$

where $\mathbf{n}$ is the outward normal of surface $\mathbf{S}$.

There is also a classical technique used to evaluate the force by computing the time derivative of the linear impulse (external flow around one body):

$$\frac{\mathbf{F}}{\rho} = -\frac{\mathrm{d}\mathbf{I}}{\mathrm{d}t} \tag{6}$$

where ρ is the density and $\mathbf{I}$ is defined by

$$\mathbf{I} = \frac{1}{2}\int_V \mathbf{x}\times\boldsymbol{\omega}\,\mathrm{d}V \tag{7}$$

3. NUMERICAL IMPLEMENTATION

The governing equations as well as the boundary conditions presented in the previous section are globally coupled. A finite volume method is used to solve the vorticity transport equations, while the boundary conditions are implemented by using vortex sheets on the surface of the solid body. The velocity evaluation is carried out using a combination of two methods, the direct integration using numerical integral and the indirect integration using fast summation.

3.1. Finite volume scheme

The vorticity transport equation (3) can be written in the integral form:

$$\frac{\partial}{\partial t}\iiint_V W\,\mathrm{d}V + \iint_S \mathbf{F}(W)\cdot\mathbf{n}\,\mathrm{d}S = 0 \tag{8}$$

where $\mathbf{n}$ is the unit normal vector of the surface S of the control volume V.

$$W = [\omega_1 \;\; \omega_2 \;\; \omega_3]^{\mathrm{T}} \tag{9}$$

DOI: 10.1002/fld

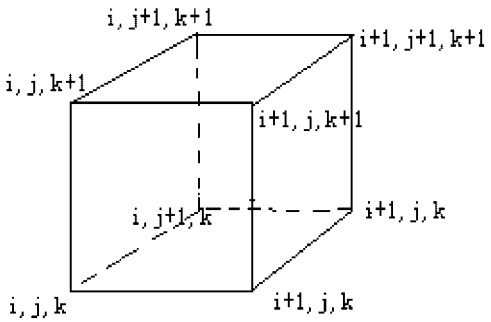

Figure 1. The typical hexahedral cell in the domain.

$$\mathbf{F}(W) = \begin{bmatrix} F_1(W) \\ F_2(W) \\ F_3(W) \end{bmatrix}^{\mathrm{T}} \tag{10}$$

$$F_1(W) = \begin{bmatrix} -v\dfrac{\partial \omega_1}{\partial x} \\ u_1\omega_2 - u_2\omega_1 - v\dfrac{\partial \omega_2}{\partial x} \\ u_1\omega_3 - u_3\omega_1 - v\dfrac{\partial \omega_3}{\partial x} \end{bmatrix} \tag{11}$$

$$F_2(W) = \begin{bmatrix} u_2\omega_1 - u_1\omega_2 - v\dfrac{\partial \omega_1}{\partial y} \\ -v\dfrac{\partial \omega_2}{\partial y} \\ u_2\omega_3 - u_3\omega_2 - v\dfrac{\partial \omega_3}{\partial y} \end{bmatrix} \tag{12}$$

$$F_3(W) = \begin{bmatrix} u_3\omega_1 - u_1\omega_3 - v\dfrac{\partial \omega_1}{\partial z} \\ u_3\omega_2 - u_2\omega_3 - v\dfrac{\partial \omega_2}{\partial z} \\ -v\dfrac{\partial \omega_3}{\partial z} \end{bmatrix} \tag{13}$$

The 3D computational domain is divided into hexahedral cells as shown in Figure 1, and a system of differential equations is obtained by applying Equation (8) to each cell separately.

DOI: 10.1002/fld

Let the values of the quantities associated with each cell be denoted by i, j, k (values at the cell centre). For each cell Equation (8) can be presented as the form

$$\frac{\mathrm{d}}{\mathrm{d}t}(h_{ijk}W_{ijk}) + Q(W)_{ijk} = 0 \tag{14}$$

where h is the volume of the cell and Q is the flux term.

$$\begin{aligned} Q(W)_{ijk} = Q_{ijk} &+ \mathbf{F}\cdot\mathbf{S}|_{i+1/2,j,k} - \mathbf{F}\cdot\mathbf{S}|_{i-1/2,j,k} \\ &+ \mathbf{F}\cdot\mathbf{S}|_{i,j+1/2,k} - \mathbf{F}\cdot\mathbf{S}|_{i,j-1/2,k} + \mathbf{F}\cdot\mathbf{S}|_{i,j,k+1/2} - \mathbf{F}\cdot\mathbf{S}|_{i,j,k-1/2} \end{aligned} \tag{15}$$

where $\mathbf{S}|_{i+1/2,j,k}$ is the normal area on i direction of the interface between cell (i, j, k) and cell $(i + 1, j, k)$.

A second-order Adams–Bashforth scheme is used to advance in time:

$$(\omega_i h)^{n+1}_{i,j,k} = (\omega_i h)^{n}_{i,j,k} + \frac{\Delta t}{2}[3Q_{i,j,k}(t_n, \omega_i^n, \mathbf{u}^n) - Q_{i,j,k}(t_{n-1}, \omega_i^{n-1}, \mathbf{u}^{n-1})] \tag{16}$$

The diffusive flux term is discretized using central differential scheme. For the convective terms, a third-order QUICK (quadratic upwind interpolation for convective kinematics) [12] scheme is used.

3.2. Vorticity boundary conditions

The vorticity boundary conditions employed in the present paper are based on vortex sheet method [10, 13]. A piecewise-continuous vortex sheet is used to replace the body surfaces in order to cancel the slip velocity. The strength of the sheet is obtained from a Fredholm boundary integral equation of the second kind:

$$\frac{1}{2}\boldsymbol{\Delta\gamma}(\mathbf{x})\times\mathbf{n} + \frac{1}{4\pi}\int_{\mathbf{S}} \frac{\mathbf{1}}{|\mathbf{x}-\mathbf{x}'|^{\mathbf{3}}}\cdot(\mathbf{x}-\mathbf{x}')\times\boldsymbol{\Delta\gamma}(\mathbf{x}')\,\mathrm{d}\mathbf{x}' = u_{\mathrm{slip}} \tag{17}$$

where $\Delta\boldsymbol{\gamma}(\mathbf{x})$ is the strength of the vortex sheet and $\mathbf{u}_{\mathrm{slip}}$ is the slip velocity on the surface.

To implement this boundary condition, the body surface is discritized using the surface mesh as vortex panels. The slip velocity at each panel control point is induced by the free stream, surface panels and all wake vortex elements within the flow. The vortex strength $\Delta\boldsymbol{\gamma}(\mathbf{x})$ is computed by solving a linear system after evaluating the slip velocity on all the panels. Then the vortex flux to be emitted into the flow can be obtained as

$$\boldsymbol{\nu}\frac{\partial\boldsymbol{\omega}}{\partial\mathbf{n}} = \frac{\boldsymbol{\Delta\gamma}(\mathbf{x})}{\Delta t} \tag{18}$$

3.3. Velocity evaluations

3.3.1. Direct integration method. In the present method, the vorticity field is represented by a structured grid system consisting of a number of hexahedral elements. The evaluation of Biot–Savart integral is required to calculate the velocity field. Therefore, a robust and accurate algorithm is needed for the integration over a hexahedral element. Suh [11] proposed an elegant method for the evaluation of Biot–Savart integral in both two and three dimensions. It transforms the volume integral into line integrals based on Gauss and Stokes integral theorems and can be applied to

DOI: 10.1002/fld

elements with arbitrary number of faces (sides). However, after applying this approach to the current study, it was found that some limitations need to be imposed onto the original expressions presented in [11], otherwise, in some cases, one or two terms would produce infinite values. The other change to the original expressions is that the vorticity distribution within the elements is simplified to be uniform in this study rather than Suh's linear distribution.

According to the Biot–Savart law, the induced velocity due to a vorticity distribution over an element bounded by planar panels can be expressed as

$$\mathbf{u} = \frac{1}{4\pi}\nabla \times \iiint_V \frac{\boldsymbol{\omega}}{r}\,\mathrm{d}V = \frac{1}{4\pi}\iiint_V \boldsymbol{\omega} \times \nabla\left(\frac{1}{r}\right)\mathrm{d}V = \frac{1}{4\pi}\boldsymbol{\omega} \times \mathbf{n}_j \sum_{j=1}^{N_s} \iint_{S_j} \frac{1}{r}\,\mathrm{d}S \tag{19}$$

where N_s is the total number of planar panels bounding the element and $\mathbf{n}_j$ is the unit normal of the jth panel.

Now

$$\frac{\mathbf{1}}{r} = \mathbf{e}_n \cdot (\nabla \times \mathbf{B}) \tag{20}$$

$$\mathbf{B} = \frac{\mathbf{e}_n \times \mathbf{r}}{\mathbf{r} + \mathbf{e}_n \cdot \mathbf{r}} \tag{21}$$

where $\mathbf{e}_n = \pm\,\mathbf{n}$ such that $e = \mathbf{e}_n \cdot \mathbf{r} \geqslant 0$ then

$$\iint_{S_j} \frac{1}{r}\mathrm{d}S = \pm \iint_{S_j} \mathbf{n} \cdot (\nabla \times \mathbf{B})\,\mathrm{d}S = \pm \oint_C \mathbf{B}\,\mathrm{d}C \tag{22}$$

where C is the perimeter of the planar panel. For a quadrilateral panel, it can be expressed as

$$\oint_C \mathbf{B}\,\mathrm{d}C = \sum_{k=1}^{4} \int_{l_k} \mathbf{B} \cdot \mathbf{l}_k\,\mathrm{d}l \tag{23}$$

where $\mathbf{l}_k$ is the unit directional vector of side l_k.

For the evaluation of the line integrals, a local coordinate system (ξ, η) is used in the panel, as shown in Figure 2.

Now we have

$$\mathbf{r} = \mathbf{r}_k + \xi \mathbf{l}_k \tag{24}$$

and

$$r = \sqrt{r_k^2 - 2\xi_p \xi + \xi^2} \tag{25}$$

because $(\mathbf{n} \times \mathbf{r}) \cdot \mathbf{l}_k = \mathbf{r} \cdot (\mathbf{l}_k \times \mathbf{n}) = \mathbf{r}_k \cdot \mathbf{p}_k$.

Hence,

$$\int_{l_k} \mathbf{B} \cdot \mathbf{l}_k\,\mathrm{d}l = \mathbf{r}_k \cdot \mathbf{p}_k \int_0^{l_k} \frac{\mathrm{d}\xi}{\sqrt{(\xi - \xi_p)^2 + \eta_p^2 + e}} \tag{26}$$

After some manipulations, the indefinite integral in Equation (26) can be expressed as

$$\int \frac{\mathrm{d}\xi}{\sqrt{(\xi - \xi_p)^2 + \eta_p^2 + e}} = I_1 + I_2 \tag{27}$$

DOI: 10.1002/fld

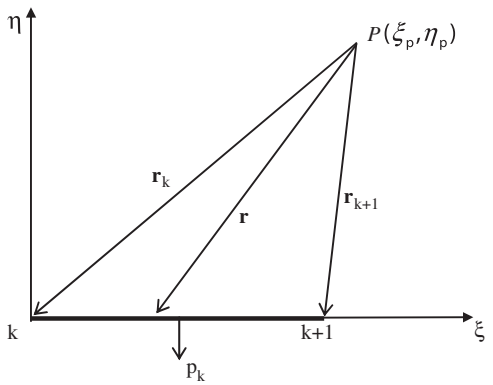

Figure 2. Definition of the local coordinate system.

where

$$I_1 = \ln \left| \frac{(l_k - \xi_p) + r_{k+1}}{r_k - \xi_p} \right| \tag{28}$$

I_2 requires some special treatment, looking at two different cases:

(1) If $\xi < \xi_p$ or $\xi > \xi_p$, for $0 < \xi < l_k$

$$I_2 = \frac{e}{\sqrt{\eta_p^2 - e^2}} \beta \tag{29}$$

where

$$\beta = \arcsin \left(\frac{\sqrt{\eta_p^2 - e^2}[\eta_p^2 l_k + e(l_k - \xi_p) r_k + e\xi_p r_{k+1}]}{\eta_p^2 (e + r_{k+1})(e + r_k)} \right) \tag{30}$$

(2) If $\xi < \xi_p$ and $0 < \xi < \xi_p$, for $0 < \xi_p < l_k$ or $\xi > \xi_p$ and $\xi_p < \xi < l_k$, for $0 < \xi_p < l_k$

$$I_2 = \frac{e}{\sqrt{\eta_p^2 - e^2}} (\pi - \beta) \tag{31}$$

3.3.2. Indirect integration method. The direct integration method presented in the last section requires calculations of 12 logarithmic and angular functions for a single hexahedral element. For a large number of elements, the time required for direct integration becomes excessive. Therefore, a fast summation algorithm is used in this paper, based on the Taylor expansion [5, 6].

A hierarchical grid system is firstly introduced to generate a box tree. The root of the tree is the single box containing all the vortex particles in the flow. Then each box of the tree is divided into two offspring boxes with equal size by cutting the longest side of the box. This process continues until the number of vortex particles in the smallest box, the top of the box tree, is less than a prescribed value.

DOI: 10.1002/fld

For points **y** in a single box τ centred at $\mathbf{y}_\tau$, their influence at a fix point **x** can be expressed as

$$f(x, y) = \frac{x - y}{|x - y|^3} = \sum_{|k| \leqslant \lambda - 1} \frac{1}{k!} D_y^k f(x, y)_{y = y_\tau} (y - y_\tau)^k \tag{32}$$

where

$$k = (k_1, k_2, k_3), \quad |k| = k_1 + k_2 + k_3, \quad k! = k_1! k_2! k_3!$$

$$D_y^k = \partial^{|k|} / \partial y_1^{k_1} \partial y_2^{k_2} \partial y_3^{k_3}, \quad y^k = y_1^{k_1} y_2^{k_2} y_3^{k_3}$$

The degree of its Taylor polynomial is $\lambda - 1$.

Then the calculation of the velocity $\mathbf{u}(\mathbf{x})$ at point **x** is given by

$$u(x) = -\frac{1}{4\pi} \sum_{|k| \leqslant \lambda - 1} a_k(x, y_\tau)[(x_2 A_\tau^k - B_\tau^k - x_3 C_\tau^k + D_\tau^k), \tag{33}$$

$$(x_3 E_\tau^k - F_\tau^k - x_1 A_\tau^k + G_\tau^k), (x_1 C_\tau^k - H_\tau^k - x_2 E_\tau^k + I_\tau^k)] \tag{34}$$

The sums in the above equations are evaluated for all boxes τ and indices k before the velocity calculation and in parallel with the vortex sorting and grid generation process [14].

4. FLOW PAST A SPHERE

The hybrid vortex method presented in previous sections is utilized for the computation of flow past a sphere. The flow is started impulsively at various Reynolds numbers (Re) (100, 200, and 300) with two different flow field resolutions (medium and high). The flow variables are normalized using the diameter of the sphere and the free-stream velocity, which is oriented in the positive x direction. A single-block structured grid (Figure 3) has been created around the sphere. The number of hexahedral elements varies from a resolution of 36 000 to 64 000 and 108 000. The radius of the sphere was taken as $R_0 = 0.5$, and the outer radius of the domain was $R_1 = 5.0$.

An impulsive start of the flow is initialized by computing the potential flow past the sphere body using the vortex sheet method (Equation (17)). The vorticity associated with the surface slip is then distributed to the boundary cells through the diffusion process (Equation (18)). The surface slip velocity is recomputed at the beginning of the next time step to provide a continuing source of vorticity. The calculation was carried out on a DELL PRECISION 470 workstation with two Intel Xeon (TM) CPU.

The flow past a sphere behaves differently when Reynolds number (Re) changes. In the range of Re<210–212 [15, 16], the flow remains steady and axisymmetric although separated. Above that, if Re<270, the flow remains steady but is no longer axisymmetric. When Re>290 [15], the flow becomes unsteady but still retains time periodicity and planar symmetry. Two (100 and 200) of the

DOI: 10.1002/fld

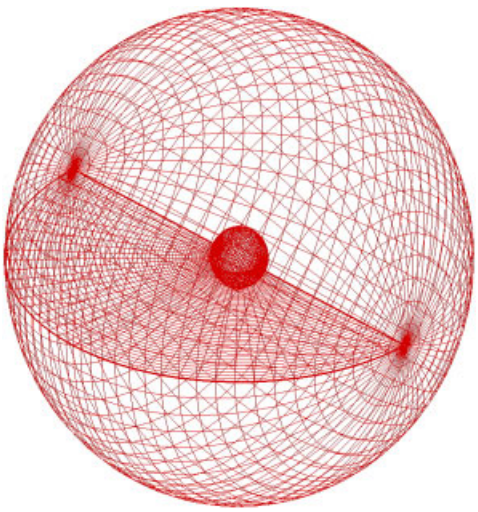

Figure 3. The structured grid used for the sphere flow simulation.

three Reynolds numbers simulated in this study are below 210, corresponding to the axisymmetric flow. The other one (300) was used to test the potential of the hybrid vortex method, but due to the capability of the workstation, only the early stage of the unsteady flow has been simulated.

4.1. Force coefficient history

Figures 4–6 show the drag coefficients $Cd = D/(0.5\rho U^2 \pi R^2)$ plotted as a function of time, at three Reynolds number 100, 200, and 300. The drag coefficient results are compared with the values from the Schiller–Naumann formula [17] $Cd = (24/Re)[1 + 0.15\,Re^{0.687}]$ and the results from Johnson and Patel [15]. The drag coefficients are observed to have a quick decline from the initial overshoot in the range $0<t<0.5$, then to approach a steady-state average value. The curves of the drag coefficient appear to exhibit more fluctuation when Re increases.

4.2. Flow characteristics

Figures 7–9 show the streamlines in the x–y plane at Reynolds number 100, 200, and 300. For all these three Reynolds numbers, the flow is seen to separate from the surface of the sphere and form a separation bubble in the wake. A clear axisymmetric flow pattern can be seen in both flows at $Re = 100$ and 200, with the only difference being the length of the separation bubble and the position of the vortex. However, for $Re = 300$, even at the early stage of simulation, the flow has started to show asymmetrical characteristics and unsteadiness. This feature can be seen more clearly from a three-dimensional view shown in Figure 10.

In Figure 11, the vorticity $|\omega|$ contours in the x–y plane at several instances for $Re = 200$ are presented. Again, the axisymmetric flow characteristics can be observed through the development of the separated flow.

DOI: 10.1002/fld

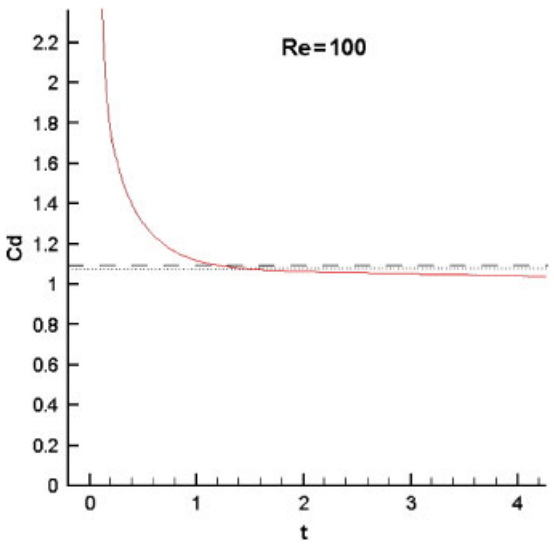

Figure 4. Drag coefficient comparison for the flow past a sphere at $Re = 100$, showing computed results (solid line), Schiller–Naumann formula (dashed line), and results from Johnson and Petel (dotted line).

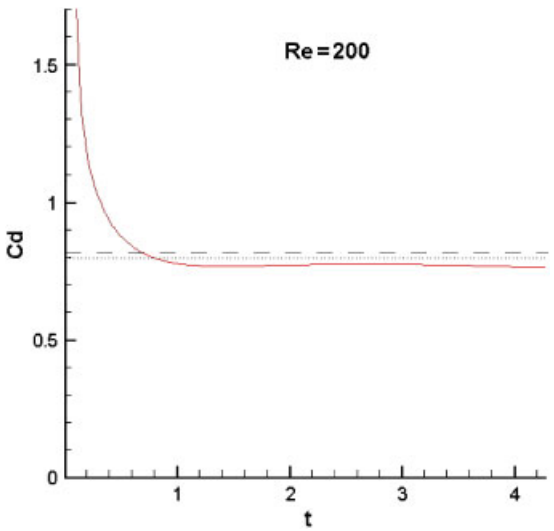

Figure 5. Drag coefficient comparison for the flow past a sphere at $Re = 200$, showing computed results (solid line), Schiller–Naumann formula (dashed line), and results from Johnson and Petel (dotted line).

4.3. Effects of numerical parameters

In Figures 12 and 13, the effect of numerical parameters, in terms of time steps and grid resolution, on total drag coefficients is presented for $Re = 300$. From Figure 12, the sensitivity of the time step to the computation of drag coefficient can be observed. The use of smaller time steps, $dt = 0.005$

DOI: 10.1002/fld

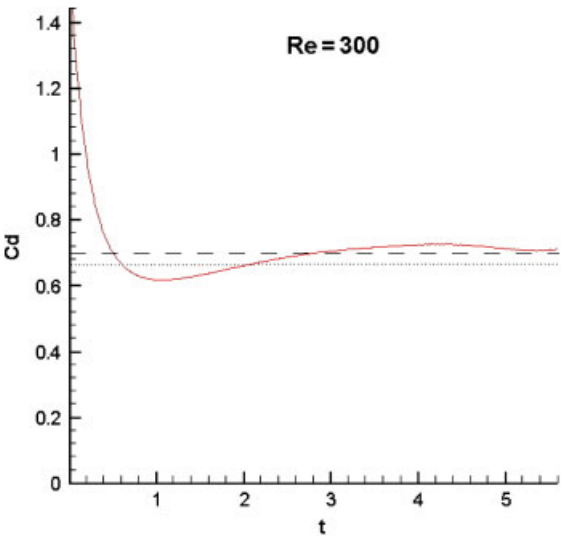

Figure 6. Drag coefficient comparison for the flow past a sphere at $Re = 300$, showing computed results (solid line), Schiller–Naumann formula (dashed line), and results from Johnson and Petel (dotted line).

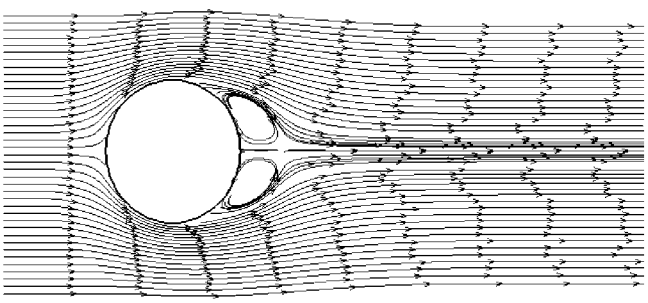

Figure 7. Streamlines of sphere flow in the $x-y$ plane at $Re = 100$.

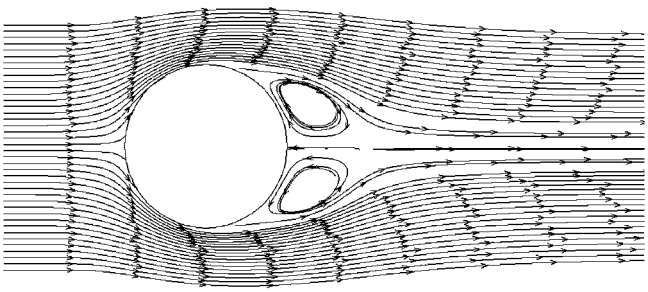

Figure 8. Streamlines of sphere flow in the $x-y$ plane at $Re = 200$.

DOI: 10.1002/fld

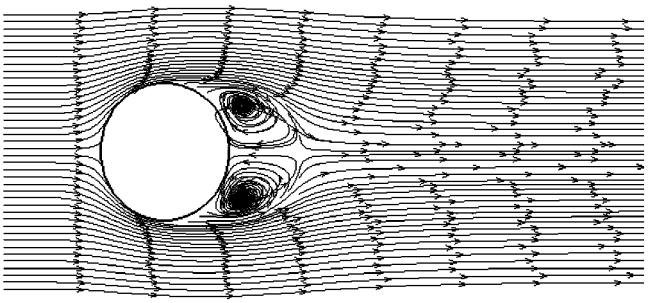

Figure 9. Streamlines of sphere flow in the x–y plane at $Re = 300$.

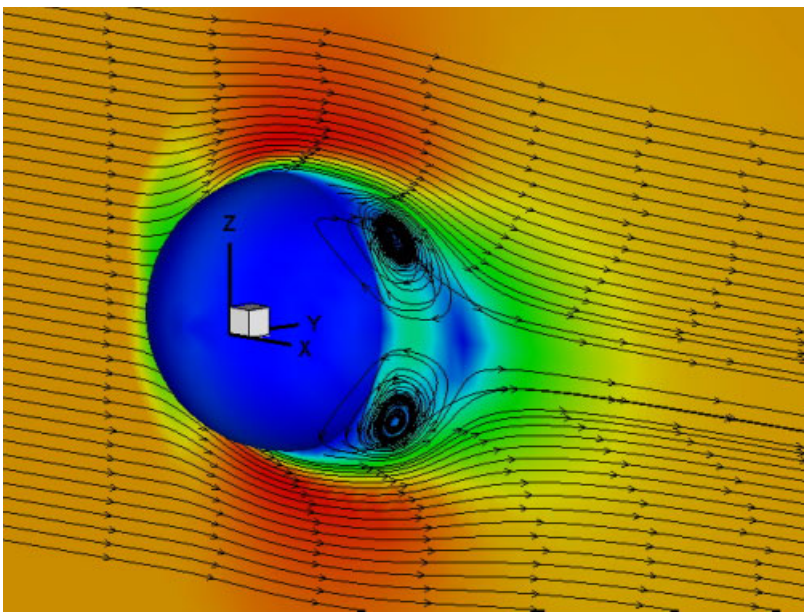

Figure 10. Three-dimensional view of the streamlines of sphere flow in the x–y plane at $Re = 300$. The velocity contour is also shown.

and 0.0025, produced nearly identical drag values near the immediate time region ($t = 0+$) after the impulsive start. The use of the moderate time step, $dt = 0.01$, appears to be less accurate, although it is preferred for the long-term simulation.

To evaluate the effect of grid resolution, three grids, namely Grid1 (total grid number is 36 000) and Grid2 (total grid number is 64 000) and Grid3 (total grid number is 108 000), are used separately for the simulation of a flow at $Re = 300$. In Figure 13, it can be seen that the coarser grid, Grid1, causes larger fluctuation in the drag force. At some points around $t = 3.5$, unexpected disturbances appeared that may trigger an earlier oscillation in the later stage of simulation. The result from the use of Grid3 shows no significant change compared with the use of Grid2, indicating at these two resolutions, the simulations were converged.

DOI: 10.1002/fld

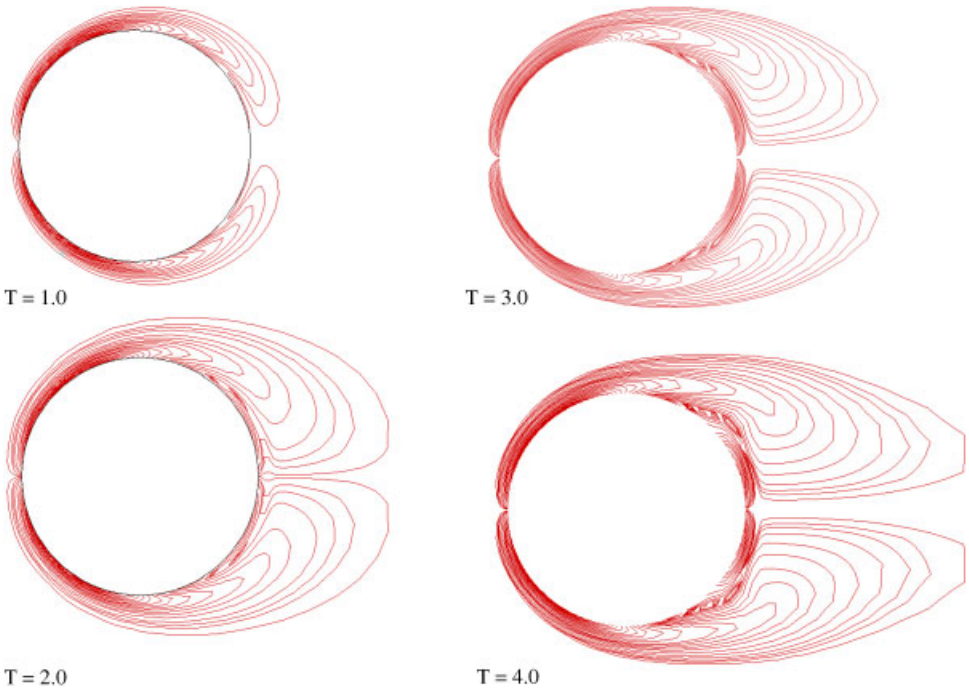

Figure 11. The vorticity contours at four instances of time at $Re = 200$.

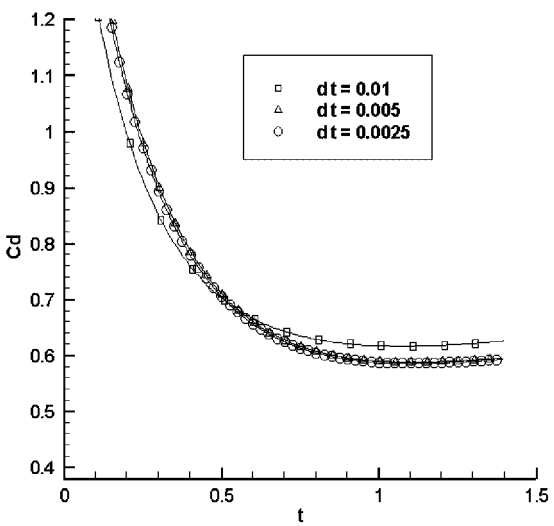

Figure 12. Sensitivity of time step on the drag coefficients at $Re = 300$.

DOI: 10.1002/fld

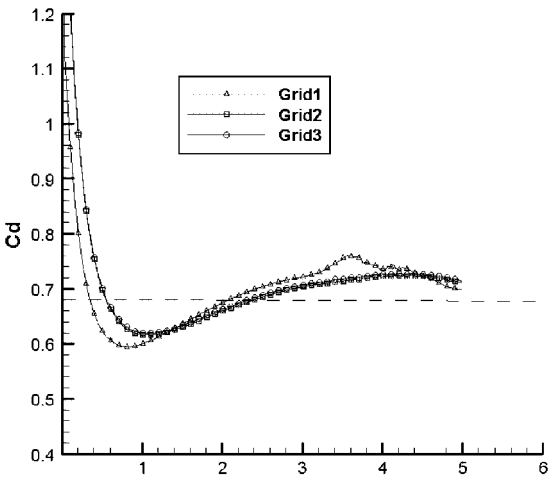

Figure 13. The effect of grid resolution on the drag coefficient at $Re = 300$.

5. CONCLUSIONS

A hybrid vortex method is proposed in this paper. This approach extends Lagrangian vorticity-based methods by using a hexahedral grid system in place of the method of overlapping vortex particles/blobs. The finite volume method is used to solve the three-dimensional incompressible Navier–Stokes equations in conjunction with the use of a modified Biot–Savart formula for the calculation of flow velocity. This hybrid approach can guarantee the conservation of the vorticity and mass within the entire flow domain including the prevention of the bleeding of vorticity over the surface of an immersed body.

A closed-form formula, initially proposed by Suh [11], has been used with essential modifications to accomplish the numerical integration over the surfaces of a hexahedral element for the calculation of flow velocity. A fast algorithm is also used to accelerate the process of velocity evaluation.

The work presented in this paper is the preliminary research and development of this hybrid approach. The initial application of the method to the case of a sphere at low *Re* indicates that predicted drag and flow patterns are in line with the expectations. Future works will concentrate on extending the capability of this code through implementations of advanced differential schemes in conjunction with parallization techniques.

ACKNOWLEDGEMENTS

The authors wish to acknowledge the financial supports from EPSRC.

REFERENCES

1. Leonard T. Computing three-dimensional incompressible flows with vortex elements. *Annual Review of Fluid Mechanics* 1985; **17**:523.
2. Marshall JS, Grant JR, Gossler AA, Huyer SA. Vorticity transport on a Lagrangian tetrahedral Mesh. *Journal of Computational Physics* 2000; **161**:85–113.

DOI: 10.1002/fld

3. Cottet G-H, Koumoutsakos PD. *Vortex Methods: Theory and Practice*. Cambridge University Press: Cambridge, 2000.
4. Winckelmans GS. Vortex methods. *Encyclopaedia of Computational Mechanics*, vol. 3. Wiley: New York, 2004.
5. Van Dommelen L, Rundensteiner EA. Fast, adaptive summation of point forces in the two-dimensional Poisson equation. *Journal of Computational Physics* 1989; **83**:126–147.
6. Draghicescu CI, Draghicescu M. A fast Algorithm for vortex blob interaction. *Journal of Computational Physics* 1995; **116**:69–78.
7. Clarke NR, Tutty OR. Construction and validation of a discrete vortex method for two-dimensional in compressible Navier–Stokes equations. *Computers and Fluids* 1994; **23**:751–783.
8. Koumoutsakos P, Leonard A. High-resolution simulations of the flow around an impulsively started cylinder using vortex methods. *Journal of Fluid Mechanics* 1995; **296**:1–38.
9. Shankar S, Van Dommelen L. A new diffusion procedure for vortex methods. *Journal of Computational Physics* 1996; **127**:88–109.
10. Ploumhans P, Winkelmans GS, Salmon JK, Leonard A, Warren MS. Vortex methods for direct numerical simulation of three-dimensional bluff body flows: application to the sphere at $Re = 300$, 500 and 1000. *Journal of Computational Physics* 2002; **178**:427–463.
11. Suh J-C. The evaluation of the Biot–Savart integral. *Journal of Engineering Mathematics* 2000; **37**:375–395.
12. Leonard BP. A stable and accurate convection modelling procedure based on quadratic upstream interpolation. *Computer Methods in Applied Mechanics and Engineering* 1979; **19**:59–98.
13. Koumoutsakos P, Leonard A, Pepin F. Boundary conditions for viscous vortex methods. *Journal of Computational Physics* 1994; **113**:52–61.
14. Qian L. Towards numerical simulation of vortex-body interaction using vorticity-based methods. *Ph.D. Thesis*, University of Glasgow, Glasgow, 2001.
15. Johnson TA, Patel VC. Flow past a sphere up to a Reynolds number of 300. *Journal of Fluid Mechanics* 1999; **378**:19.
16. Tomboulides G, Orszag SA. Numerical investigation pf transitional and weak turbulent flow past a sphere. *Journal of Fluid Mechanics* 2000; **416**:45.
17. Schiller L, Naumann A. Über die grundlegenden Berechungen bei der Schwerkraftaubereitung. *Vereines Deutscher Ingenieure* 1933; **77**:318.

DOI: 10.1002/fld